Int. J. Metrol. Qual. Eng. **7**, 305 (2016)

DOI: 10.1051/ijmqe/2016015

Available online at:
www.metrology-journal.org

Absolute falling ball viscometer, adapted to the low viscosities of liquids

Patrick Ballereau*, Daniel Truong, and Adriana Matias

Joint Metrology Laboratory LNE-CNAM, 1 rue Gaston Boissier, 75724 Paris Cedex 15, France

Received: 9 September 2016 / Accepted: 13 September 2016

Abstract. The Joint Metrology Laboratory LNE-CNAM had an absolute falling ball viscometer, which was operating only at laboratory temperature. Its development ceased in 2005 but resumed in 2010, the aim being to make it operational, by regulating, at first, its temperature between 15 °C and 50 °C, and adapting it to low liquid viscosities up to a value of 15 mPa s. This study aims to approach the viscosity of fuels or biofuels. Their low viscosity requires the use of a small-diameter ball. A silicon ball with 0.48 mm diameter was selected. The small diameter of this ball mandated the design and the construction of a gripper. This gripper uses the following microsystem-specific technique: the adhesion by van der Waals forces. The operation of this gripper is described in this article. It was designed to perform the following dual function: freeing the ball into the liquid at the top, then recovering it at the bottom of the viscometer, in order to reposition and prepare it for another release.

Keywords: absolute falling ball viscometer / biofuel / microsystem / rheology / yield stress

1 Introduction

Given the necessary global reduction of greenhouse gas emissions and a compulsory saving in fossil fuel energy consumption, the use of biofuels [1] is required. European legislators have taken measures in this regard [2].

The viscosity of biofuels and of their blends with fossil fuels is not well known, despite the fact that it is an essential feature, for their transport in pipelines. Like fossil fuels, these biofuels have low viscosities (some mPa s), and according to TRAPIL, a company transporting oil via pipeline, they are used in temperature conditions that can vary from −10 °C up to +50 °C, and in variable pressure conditions going from 0.1 MPa up to 10 MPa.

The viscosity that varies according to temperature and pressure is therefore an important parameter in the transport of fuels and biofuels.

The project aims to operationalize a falling ball viscometer in order to be able to measure the viscosities of fuels and biofuels blends over a temperature range from −10 °C up to +50 °C and also with a pressure up to 10 MPa. Initially, this project is limited to a temperature range from +15 °C up to +50 °C and only at atmospheric pressure.

The ultimate goal of this research is to operationalize a falling ball viscometer so that it becomes an absolute reference, by linking the dynamic viscosity of the following different quantities: mass, length, and time.

* Corresponding author: patrick.ballereau@cnam.fr

2 State of the art

Several studies on the falling ball viscometers were conducted with Newtonian fluids [3], and wealthy fluids in suspended particles [4].

In the metrology field, the work conducted at the National Metrology Institute of Japan (NMIJ) led to the construction of an absolute viscometer for measurements at high pressures (500 MPa) [5]. The NMIJ also decided in 1998 [6] to build an absolute falling ball viscometer, in order to determine a new value of water viscosity, with a new uncertainty. The progress of both the NMIJ and LCM/LNE-CNAM viscometers was presented in the CCM Working Group on Viscosity at BIPM, in May 2011 [7,8].

3 Scientific and technical aim

In 2005, LCM/LNE-CNAM had a falling ball viscometer, which was developed and studied by Brizard [9] during his thesis.

The photograph of Figure 1 shows the measurement cell, which was operating only at laboratory temperature.

The metrological study carried out during this thesis demonstrated that it is possible to obtain relative uncertainties of 10^{-3} for viscosities equal to or higher than 10 Pa s. Furthermore, the relative uncertainties of the falling ball viscometer are becoming better than those of capillary viscometers, for viscosities higher than 1 Pa s.

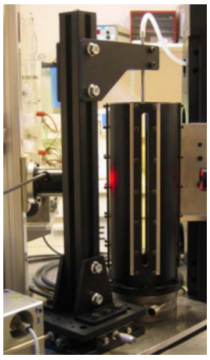

Fig. 1. Measurement cell of falling ball viscometer.

The development of this viscometer, which ceased in 2005 resumed in 2010 with the aim to adapt it to the low viscosities of biofuels, adjust it to temperatures between −10 °C and +50 °C, and build a small-volume cell to perform intercomparisons.

The viscometer was modified in three main stages:
- *adaptation to low viscosities* (of biofuels) using specific balls;
- *adaptation to controlled temperatures* through the development of a thermostatic bath;
- *construction of a cell for intercomparisons.*

3.1 Project for adapting the viscometer to low viscosities

3.1.1 Order of magnitude for biofuel viscosity

The first results achieved by LCM/LNE-CNAM regarding biofuels in terms of kinematic viscosity and density were presented during the ENG09–Biofuel (European funded programme by EURAMET) annual meeting in Helsinki [10] in January 2011.

The kinematic viscosity measurements were performed with capillary viscometers while density measurements were performed with pycnometers.

Note: The kinematic viscosity ν is defined as the ratio of the dynamic viscosity η in relation to density ρ.

$$\nu = \frac{\eta}{\rho}. \tag{1}$$

The evolutions of kinematic viscosity and density according to temperature, of two pure biofuels made from rapeseed and soybean, are shown in Figures 2 and 3.

At 20 °C, the dynamic viscosity of these biofuels is of the order of 6 mPa s, which is 6 times higher than that of water.

3.1.2 Reminding the principle of the falling ball viscometer

The dynamic viscosity η of a liquid is obtained from the measurement of the fall velocity U_∞, of d diameter and ρ_b density ball into this same liquid featuring ρ_1 density.

The dynamic equilibrium equation of the ball gives the following relation:

$$\eta = \frac{d^2}{18U_\infty}(\rho_b - \rho_l)g, \tag{2}$$

g, gravity acceleration.

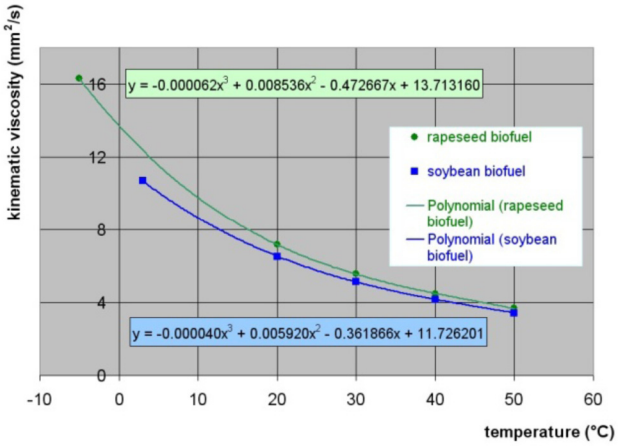

Fig. 2. Evolution of kinematic viscosity depending on temperature [10] (at atmospheric pressure).

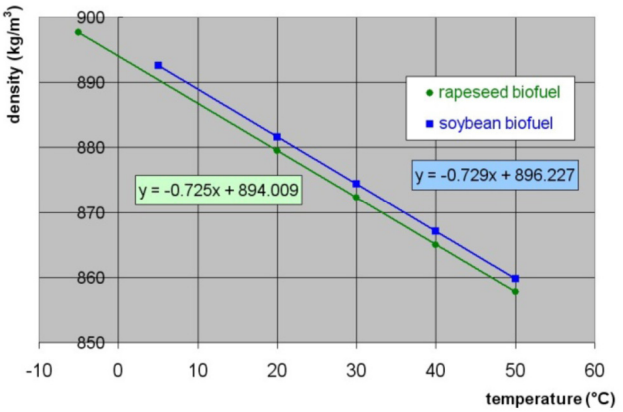

Fig. 3. Evolution of density depending on temperature [10] (at atmospheric pressure).

This relationship was obtained using the Stokes' formula (which comes from Stokes' equation) regarding the aerodynamic drag F_{stokes} (we explain this law in the paragraph titled "correction of the Reynolds effect":

$$F_{\text{Stokes}} = 6\pi\eta U_\infty d, \tag{3}$$

knowing that the formula involves the following two hypotheses:

First hypothesis (wall effect):

The ball falls into a dimensional infinite medium, which means that the ball moves in a cylinder of infinite D diameter, that is to say:

$$\frac{d}{D} \to 0. \tag{4}$$

In practice, D is a finite dimension (for this cell, $D = 99.61$ mm).

However, it is possible to introduce a k_1 correction coefficient, depending on d/D in Stokes' formula.

Second hypothesis (Reynolds effect):

The Reynolds number R_e must tend to 0.

$$R_e \to 0, \tag{5}$$

with

$$R_e = \frac{\rho_l U_\infty d}{\eta}. \tag{6}$$

For non-zero Reynolds numbers but representing small values, it is possible to introduce a second correction factor k_2 depending on R_e in Stokes' formula.

The dimensional analysis demonstrates that the drag force F_x may take the following form:

$$F_x = F_{\text{Stokes}} \times f\left(\frac{d}{D}\right) \times f(R_e). \tag{7}$$

Hence, the equilibrium ball equation is as follows:

$$\eta = \frac{d^2}{18U_\infty}(\rho_b - \rho_1)g \times k_1\left(\frac{d}{D}\right) \times k_1(R_e). \tag{8}$$

3.1.2.1 Correction of the wall effect

Stokes' equation for a moving sphere, in cylindrical boundary conditions, was solved by Bohlin [11] in 1960. This case implies a ball that falls along the axis of symmetry of a revolution cylinder with a D diameter and a near-zero Reynolds number.

The correction function $k_1(d/D)$ is the following:

$$k_1 = 1/\left(1 - 2.10443\left(\frac{d}{D}\right) + 2.08877\left(\frac{d}{D}\right)^3 - 0.94813\left(\frac{d}{D}\right)^5 - 1.372\left(\frac{d}{D}\right)^6 + 3.87\left(\frac{d}{D}\right)^8 - 4.19\left(\frac{d}{D}\right)^{10} + \cdots\right). \tag{9}$$

Its validity field is limited to the following:

$$\frac{d}{D} \prec 0.6. \tag{10}$$

3.1.2.2 Correction of Reynolds' effect

Stokes' formula expresses the force applied on the moving ball in an infinite medium with $R_e \to 0$.

In general, the aerodynamic force applied on a body by a flow is equal to the sum of the integral pressure forces and the integral frictional forces around this body. These pressure and frictional forces are known when the flow around the body, which is governed by Navier–Stokes' law is also known [12–14]:

$$\underset{\text{(a)}}{\rho(\partial\vec{U}/\partial t)} + \underset{\text{(b)}}{\rho(\vec{U}\cdot\text{grad}\vec{)}\cdot\vec{U}} = \underset{\text{(c)}}{\rho\vec{g}} - \underset{\text{(d)}}{\text{grad}\vec{\cdot}p} + \underset{\text{(e)}}{\eta\nabla^2\vec{U}}. \tag{11}$$

This equation has the 5 following terms:

(a) represents the amount of unsteady acceleration per volume unit;
(b) represents the amount of advective acceleration per volume unit (the inertial forces);
(c) represents the gravity force per volume unit;
(d) represents the pressure force per volume unit; and
(e) represents the viscous forces per volume unit.

The Navier–Stokes' equation has an exact analytical solution only for simple cases, mostly regarding isovolume fluids and specific boundary conditions [15].

The nondimentionalization of this equation [16,17] produces a dimensionless number, Reynolds' number. This number characterizes the importance of inertial forces on the viscous forces. When $R_e \to 0$, the advective term disappears.

This linear equation is Stokes' equation [18].

$$\rho(\partial\vec{U}/\partial t) = \rho\vec{g} - \vec{grad}.p + \eta\nabla^2\vec{U}. \tag{12}$$

In the case of a stationary flow, the left member of the equation is zero.

Stokes' solution (1851) provides the velocity and pressure field around the sphere. These two speed and pressure fields allow to calculate the stress exercised on this sphere, in order to achieve the previously introduced Stokes' formula.

A great number of scientific books present this demonstration [19–21].

Different authors have calculated analytically the drag of the sphere, by approximation (e.g. linearization) of the advective term of Navier Stokes' equation.

The graphic in Figure 4 compares the experimental results of Liao [22] to different other analytical and experimental results (the drag force is here presented in its dimensionless form, the aerodynamic drag coefficient [23]).

3.1.3 Selection of the ball

A ball with small diameter helps achieve a low Reynolds number.

A silicon ball with a diameter of 0.48 mm was selected because of its relatively low density (2329 kg/m^3), in order to reduce the falling speed. This ball was also selected because of its dimensional (Grade 10 ISO 3290-1998 standard), thermal, mechanical and chemical characteristics. Other balls with a larger diameter 1.73 mm and 2 mm were also selected.

Regarding biodiesel with a viscosity of 6 mPa s, the fall velocity to the dynamic equilibrium is of the order of 30.3 mm/s and the Reynolds number is about 2.1.

In this configuration, it seems difficult to use directly the falling ball viscometer to measure the biofuels' viscosity.

However, if we choose a referenced oil with a viscosity of 14.9 mPa s and a density $\rho = 835$ kg/m^3 at 20 °C, the approximate values of the falling speed and the Reynolds

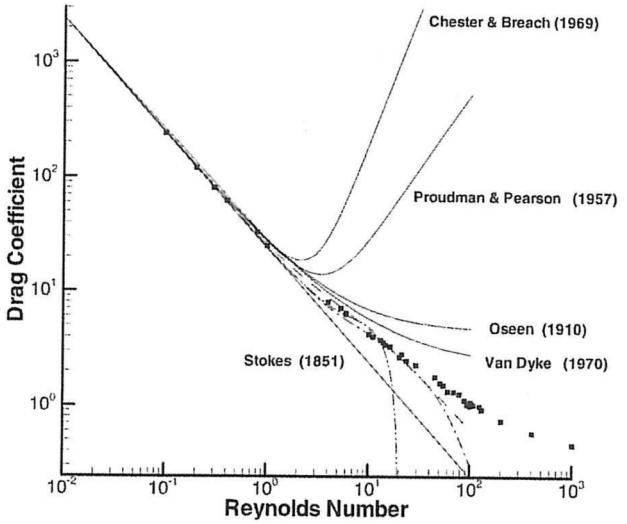

Fig. 4. Analytical results compared with the experimental results of Liao [22].

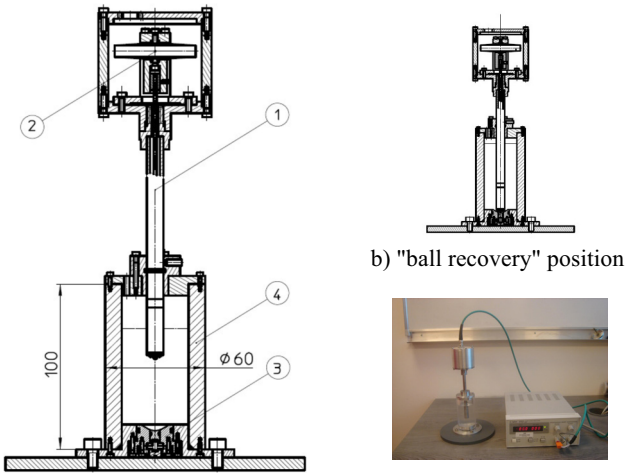

Fig. 5. Gripper mounted in the adjusting cell.

number are the following:

$$U_\infty = 12.6\text{mm/s}\ R_e = 0.34.$$

As we can see in the previous curve (Fig. 4), this Reynolds number seems acceptable.

This creates another opportunity of connection, allowing us to calibrate in absolute a referenced oil with the falling ball viscometer. This oil will then help connect viscometers that are used for biofuels.

But, the small diameter of the ball requires the construction of a gripper, suitable for releasing and recovering the ball.

3.1.4 Design and construction of a gripper

The gripping device for the ball was designed with a dual function:
– keeping the ball below the free surface of the liquid and releasing it at a given time (“ball release” phase, Fig. 5a);
– recovering the ball at the cylinder's bottom, in order to replace it under the free surface level and release it again (“ball recovery” phase, Fig. 5b).

Figure 5a shows the gripper (1), with its actuator (2) and the reception part (3). The gripper, here in “ball release” position, is installed on an adjusting cell (4) whose cylinder has reduced dimensions compared to the one of the viscometer.

Figure 5b shows the gripper in “ball recovery” position.

Figure 5c shows the gripper and its parts together with the voltage generator feeding the actuator.

Considering the small diameter of the balls, of the order of one millimeter, we realize the gripping system by using techniques suitable for microsystems, such as the adhesion by van der Walls type forces [24].

Indeed, at this scale (of the order of 1 mm), the surface forces (adhesion force) can become preponderant, ahead of the volume forces (gravity). These types of forces are interatomic and depend on the nature of the materials and the liquid at the interface.

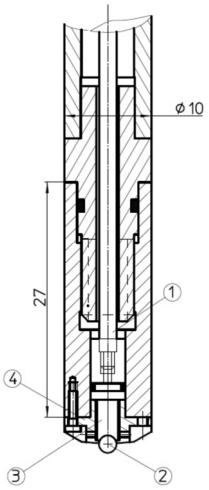

Fig. 6. Gripper extremity for a ball of 2 mm.

Explanations on the progress of the two phases, “ball release” and “ball recovery”, are presented in the following two paragraphs.

3.1.4.1 The ball release

Figure 6 shows the lower extremity of the gripper for a 2 mm ball:
– firstly, the rod (1) goes down so that the ball (2) can be grabbed through contact with the core (3) fixed on the rod;
– secondly, when to the control for lifting the rod is activated, the two surfaces in contact (ball core) are separated. In that case, the adhesion forces between the ball and the separator (4) are insufficient to keep the ball in equilibrium, and it falls.

The upward movement of the rod is caused by the contraction of the amplified piezoelectric actuator. The amplitude of the actuator's displacement is proportional to the applied voltage.

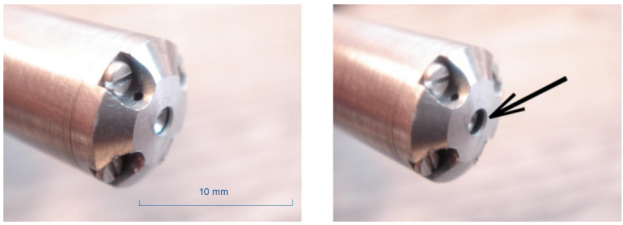

Fig. 7. "Adherence" and "release" position respectively for a ball of 2 mm.

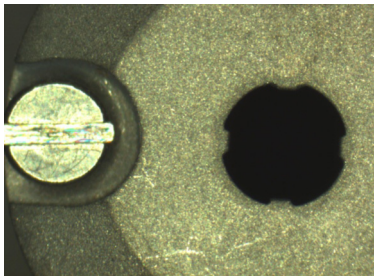

Fig. 8. Separator with notches (optical microscope).

A displacement of 0.4 mm at most is produced by a voltage of +150 V. This voltage is supplied by a generator (see Fig. 5c).

Figure 7 displays the photographs of the gripper's extremity in "adherence" and "release" position respectively, for a ball with 2 mm diameter.

By changing the core and the separator, the gripper can work for balls with a diameter of 2 mm, 1.73 mm, or 0.48 mm. All the components of the gripper are made of stainless steel.

The adhesion of the balls to their core is satisfactory thanks to the polishing performed after machining. This adjusting operation on the gripper allowed to bring the contact surfaces very close to each other, decrease their roughness, and increase the intensity of van der Walls forces.

Another type of separator with notches was tested, in order to limit the ball-separator contact forces. A photograph taken with an optical microscope, shows a separator for a ball with a 2 mm diameter. This separator is presented in Figure 8.

Figure 9 shows the ball of 0.48 mm adhering to its core, which has been removed from the gripper.

Another alternative to this type of solution was studied, by attaching the ball to the "separator" part and pushing it with a modified core, as shown in Figure 10.

3.1.4.2 Ball recovery

To recover the ball, the gripper must be lowered down to the recovery system presented in Figure 11.

Figure 12 shows the recuperator. A ball of 2 mm adhering to its core was placed just above, to give an indication about the scale.

The conical receiving part was polished by hand so that the ball can roll up to the receiver's symmetry axis, if accidentally it should not fall on the axis. Adjusting the

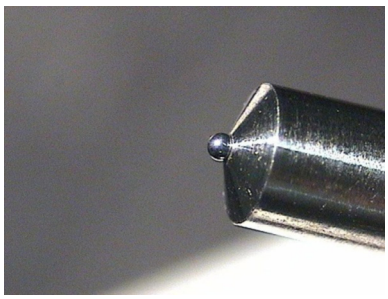

Fig. 9. Adhesion of the 0.48 mm ball to its core (optical microscope).

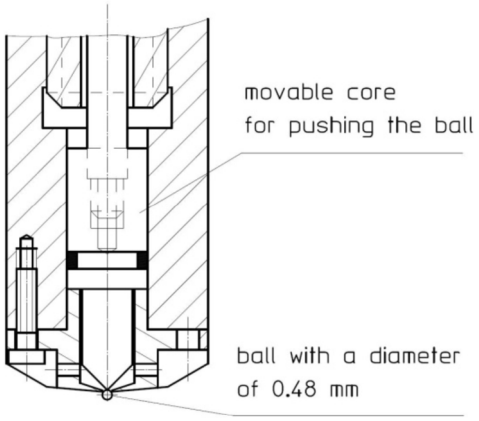

Fig. 10. Alternative solution: pushing the ball to trigger its fall.

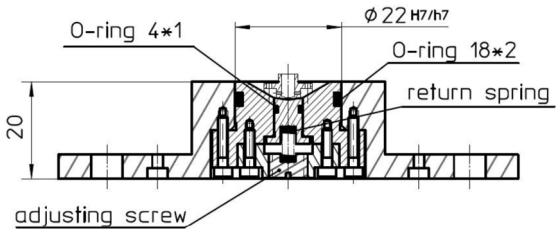

Fig. 11. Sketch of the ball recuperator.

Fig. 12. Photograph of the ball recuperator (with a ball of 2 mm diameter, to give an indication about scale).

recuperator became quite difficult because van der Walls forces increase the moment of resistance against rolling considerably.

In normal operation, the ball falls on the axis and is held in this position thanks to the conical part of the receptor, during the phase of adhesion to the core.

Then, when we lift the gripper, the ball is recovered and repositioned, in order to be released again.

Note: the central conical part of the recuperator has a return spring and is able to relocate. This system can avoid possible deformations of this one or the separator, by imposing a low contact force between the ball and the recovery.

A film showing the release and recovery of the ball in linseed oil, with a viscosity around 50 mPa s, was performed for 0.48 mm and 2 mm balls.

3.2 Adaptation to controlled temperatures (−10 °C up to +50 °C)

A thermostatic bath with optical walls was created for the immersion of the viscometer. It is presented in Figure 13. This bath is made from a semi-finished product of aluminum alloy.

This thermostatic bath has two configurations. Figure 14 shows the bath windows in "high temperatures" (a single optical borosilicate glass) and "low temperature" version (two optical made of borosilicate glass).

Both configurations were tested. First, it was tested in "high temperature" configuration, see Figure 15a.

The first tests were performed in closed circuit, because the temperature control unit has two pumps with different flow rates for the fluid input and output, thus causing fluid overflows inside the enclosure.

Operation is possible without the appearance of water vapor condensation on the windows, for temperatures between +15 °C and +50 °C.

The second configuration, reserved to low temperatures, was then tested. The bath temperature lowered down to −16.4 °C, but within prohibitive time duration, and with condensation on the windows and icing on the thermostatic bath (Fig. 15b).

This step should be continued by insulating thermally the thermostatic bath to avoid freezing the water steam and to reach −10 °C in a relatively short time.

To allow the bath to operate normally in open circuit, load losses and a liquid level maintaining system were installed.

3.3 Construction of a cell for intercomparisons and installation in the thermostatic bath

From a practical point of view, calibrations for intercomparisons are made on small volumes of liquid. Our measuring cell had a volume of 2500 ml, which was excessive.

A measuring cell of a smaller volume was thus constructed, as illustrated in Figure 16.

The cell has an inner diameter of 50 mm and a volume of 300 ml.

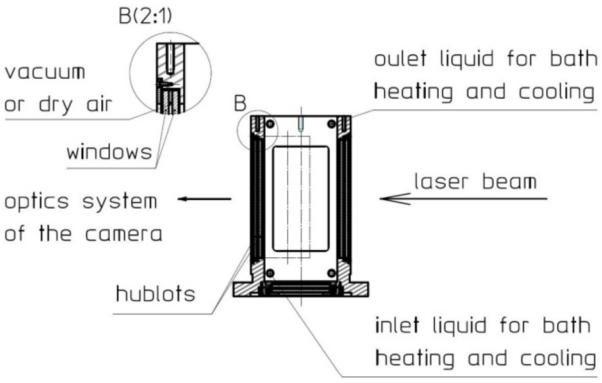

Fig. 13. Thermostatic bath.

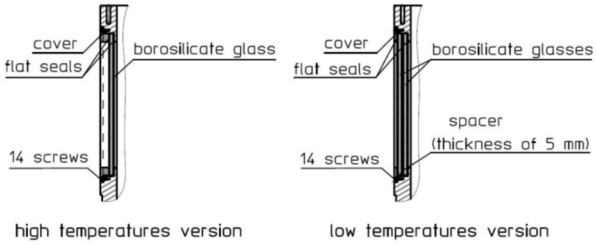

Fig. 14. Thermostatic bath windows.

a) Cooling thermostat connected to the thermostatic bath (high temperature configuration)

b) Thermostatic bath at - 16,4 °C (low temperature configuration)

Fig. 15. Thermostatic bath. (a) Cooling thermostat connected to the thermostatic bath (high temperature configuration). (b) Thermostatic bath at −16.4 °C (low temperature configuration).

Fig. 16. Cell for intercomparison.

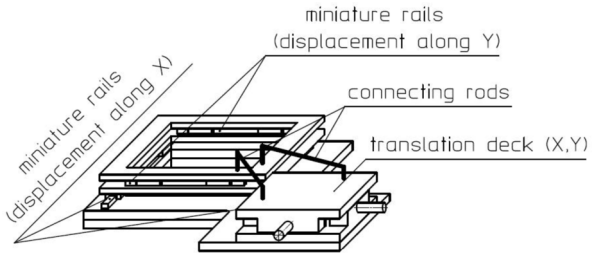

Fig. 17. Drawing in perspective of a cell displacement system.

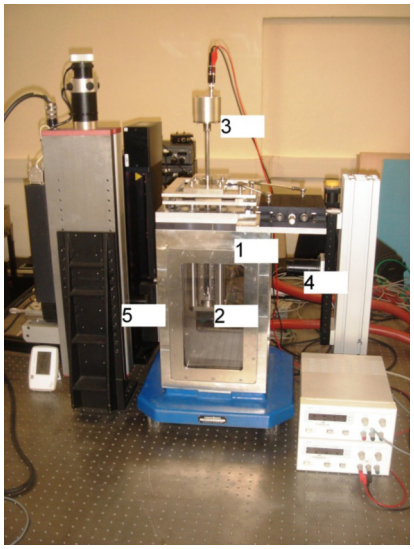

Fig. 18. Implementation of the bath in the experimental setup.

The new cell needs to be suspended at the center of a micrometric moving system, which is fixed on the upper part of the thermostatic bath to allow optical adjustments, especially the adjustment of the ball's image.

The drawing of the displacement system along the directions X and Y is presented in Figure 17.

Two parallel rails allow the movement along direction X. Two other are arranged perpendicular and allow the movement along Y.

The displacement system was built and the cell was implanted in the mounting as shown in Figure 18.

In this photograph, inside this thermostatic bath (1), we can see the following: the cell (2), the gripper (3), and the laser diode with its optical (4) before its alignment to the matrix camera (5).

After this alignment, the laser beam enlightens the ball during its course, and the shadow can be recorded by the camera. A processing of this image allows the ball speed to be calculated and the fluid viscosity to be deducted.

4 Conclusions

This work must continue with measurements on fluids of different viscosities, especially low viscosities, at standardized temperatures, for example 15 °C or 20 °C, and also 40 °C for hydrocarbons.

The thermal insulation of the thermostatic bath must continue in order to examine the operation at low temperatures up to −10 °C.

The second step is to perform a cell pressurized up to 10 MPa in order to measure the viscosity of liquids, with regard not only to the temperature, but also to the pressure on the measuring ranges, which concern the transport of biofuels.

Another advantage of falling ball viscometers in the measurement of viscosity of non-Newtonian fluids at low shear stresses, in order to determine the yield stress, is demonstrated in various publications, such as those mentioned in [25–27].

Along with this work, a research regarding the use of this experimental device as a falling ball rheometer was launched by EURAMET, as part of a European-funded research program, which is called ENG59-NNL.

This three-year program began on 1st May 2014. It is introduced on the website www.eng59-rheology.eu, and covers the metrology of drilling fluids in oil wells.

References

1. E. Poitrat, Biocarburants, Techniques de l'Ingénieur, BE 8, 550v2 (2009)
2. A.L. Hantson, D. Thomas, *Enjeux technologiques et écologiques majeurs des biocarburants* (Congrès Français de Thermique, STF2010, Le Touquet, 2010)
3. S. Feng, A.L. Graham, P.T. Readon, J. Abbott, L. Mondy, Improving falling ball tests for viscosity determination, J. Fluids Eng. **128**, 157–163 (2006)
4. W.J. Milliken, M. Gottlieb, A.L. Graham, L.A. Mondy, R.L. Powel, The viscosity-volume fraction relation for suspensions of rod-like particles by falling-ball rheometry, J. Fluid Mech. **202**, 217–232 (1989)
5. K. Fujii, Y. Fujita, N. Kuramoto, Y. Kurano, K. Fujii, A study on absolute measurement of viscosity by the falling ball method for a primary viscosity standard: development of velocity measurement system for the falling ball, Thermophys. Prop. **26**, 430–432 (2005), ISSN: 0911-1743
6. Y. Fujita, N. Kuramoto, Y. Kurano, K. Fujii, A new project at NMIJ for an absolute measurement of the viscosity by the falling ball method, in *14th international conference on the properties of water and steam in Kyoto* (2004)
7. Y. Fujita, *Progress of the absolute measurements of viscosity* (CCM Working Group on Viscosity, BIPM, Sèvres, 2011)
8. P. Ballereau, P. Pinot, T. Madec, M. Megharfi, *Report on last improvements on falling ball viscometer* (CCM Working Group on Viscosity, BIPM, Sèvres, 2011)
9. M. Brizard, Développement et étude d'un viscosimètre absolu à chute de bille, thèse de doctorat, 2005
10. P. Ballereau, E. Mahé, P. Pinot, T. Madec, Density and viscosity of pure RME (rapeseed oil methyl ester) and SME (soybean oil methyl ester) at normal pressure, in *ENG09-Biofuel, annual meeting, Helsinki, January 31st* (2011)
11. T. Bohlin, On the drag on a rigid sphere moving in a viscous liquid inside a cylindrical tube, Trans. R. Inst. Tech. (Stockholm) **155**, 1–63 (1960)
12. S. Candel, *Mécanique des fluides* (éditeur Dunod, Paris, 1991)
13. P. Chassaing, *Mécanique des fluides, éléments d'un premier parcourt* (Cépadues-éditions, Toulouse, 2000), deuxième édition

14. I.L. Ryhming, *Dynamique des fluids* (Presses polytechniques universitaires romandes, Lausanne, 1991), deuxième édition
15. H. Ha Minh, *Les équations de Navier–Stokes : propriétés et application, 30ème colloque d'aérodynamique appliquée* (École centrale de Nantes, Nantes, 1993)
16. P.-L. Violet, *Mécanique des fluides à masse volumique variable* (éditeur Presses Pont et Chaussées, Paris, 1997)
17. J. Padet, *Fluides en écoulement, méthodes et modèles* (Editeur Masson, Paris, 1991)
18. G.G. Stokes, On the effect of the internal friction of fluids on the motion of a pendulum, Trans. Camb. Philos. Soc. **9**, 8–106 (1851)
19. H. Schlichting, *Boundary-layer theory* (McGraw-Hill, New York, 1979), 7th ed.
20. P.L. Viollet, J.-M. Chabard, P. Esposito, D. Laurence, Mécanique des fluides appliquées (éditeur Presses Ponts et Chaussées, Paris, 1997)
21. E. Guyon, J-P. Hulin, L. Petit, *Hydrodynamique physique* (Editions du CNRS, Meudon, 1991)
22. S.J. Liao, An analytic approximation of the drag coefficient for the viscous flow past a sphere, Int. J. Non-Linear Mech. **37**, 1–18 (2002)
23. E.A. Brun, A. Martinot-Lagarde, J. Mathieu, *Mécanique des fluides* (Dunod, Paris, 1968), tome 1
24. P. Bidault, Préhension en robotique, Automatique-Robotique, Techniques de l'Ingénieur S7765 (2003)
25. R.P. Chhabra, J.F. Richardson, *Non-Newtonian Flow and Applied Rheology* (Elsevier, Oxford, 2008), 2nd ed.
26. M. Gottlieb, Zero-shear-rate viscosity measurements for polymer solutions by falling ball viscometry, J. Non-Newtonian Fluid Mech. **6**, 97–109 (1979)
27. V. Subbaraman, R.A. Mashelkar, J. Ulbrecht, Extrapolation procedures for zero shear viscosity with a falling sphere viscometer, Rheol. Acta 10, 429–433 (1971)

Cite this article as: Patrick Ballereau, Daniel Truong, Adriana Matias, Absolute falling ball viscometer, adapted to the low viscosities of liquids, Int. J. Metrol. Qual. Eng. **7**, 305 (2016)